HHS Public Access

Author manuscript

J Biomol NMR. Author manuscript; available in PMC 2021 December 01.

Published in final edited form as:

J Biomol NMR. 2020 December ; 74(12): 673–680. doi:10.1007/s10858-020-00349-3.

Optimized Selection of Slow-Relaxing ^{13}C Transitions in Methyl Groups of Proteins: Application to Relaxation Dispersion

Vitali Tugarinov[*], **Theodoros K. Karamanos**, **G. Marius Clore**[*]

Laboratory of Chemical Physics, National Institute of Diabetes and Digestive and Kidney Diseases, National Institutes of Health, Bethesda, MD 20892-0520, USA

Abstract

Optimized selection of the slow-relaxing components of single-quantum ^{13}C magnetization in $^{13}CH_3$ methyl groups of proteins using acute (< 90°) angle ^{1}H radio-frequency pulses, is described. The optimal selection scheme is more relaxation-tolerant and provides sensitivity gains in comparison to the experiment where the undesired (fast-relaxing) components of ^{13}C magnetization are simply 'filtered-out' and only 90° ^{1}H pulses are employed for magnetization transfer to and from ^{13}C nuclei. When applied to methyl ^{13}C single-quantum Carr-Purcell-Meiboom-Gill (CPMG) relaxation dispersion experiments for studies of chemical exchange, the selection of the slow-relaxing ^{13}C transitions results in a significant decrease in intrinsic (exchange-free) transverse spin relaxation rates of all exchanging species. For exchanging systems involving high-molecular-weight species, the lower transverse relaxation rates translate into an increase in the information content of the resulting relaxation dispersion profiles.

Keywords

methyl NMR; $^{13}CH_3$ spin-system; acute angle RF pulses; methyl ^{13}C CPMG relaxation dispersion

Methyl groups serve as unique probes of molecular structure and dynamics, and as such have played an important role in NMR investigations of proteins and protein complexes yielding considerable insights into a variety of biochemical processes (Tugarinov et al. 2004; Rosenzweig and Kay 2014; Schütz and Sprangers 2020). Recently, we revisited several classes of NMR experiments targeting selectively $^{13}CH_3$-labeled methyl sites of proteins in a highly deuterated environment, focusing primarily on pulse-scheme design optimization from the perspective of both sensitivity and simplicity. In particular, we demonstrated the utility of acute (< 90°) angle ^{1}H radio-frequency (RF) pulses for more efficient and sensitive selection of ^{1}H and ^{13}C transitions belonging to the $I = 1/2$ manifolds of $^{13}CH_3$ groups,

[*]Authors to whom correspondence should be addressed: G.M.C.: mariusc@mail.nih.gov; V.T.: vitali.tugarinov@nih.gov.

Supplementary Information. Density matrix analysis of the scheme in Figure 3A leading to the derivation of optimal values of α/β ^{1}H pulse angles. 'Materials and Methods' describing NMR sample conditions and acquisition parameters of NMR experiments.

effectively reducing the complexity of a $^{13}CH_3$ spin-system to the simpler case of its AX(^{13}C-^{1}H) counterpart (Tugarinov et al. 2020a). A special case of acute angle RF pulses, the magic-angle (54.7°) ^{1}H pulse, was shown, in the case of small to intermediate sized proteins, to simplify pulse schemes and improve sensitivity of NMR experiments that quantify the amplitudes of methyl three-fold symmetry axis motions (Tugarinov et al. 2020b).

The present communication provides a further demonstration of the utility of acute angle RF pulses in methyl NMR. The pulse scheme design stems from the realization that in NMR applications targeting single-quantum (SQ) ^{13}C transitions in a $^{13}CH_3$ methyl group for quantitative measurements of methyl ^{1}H-^{13}C residual dipolar couplings in the indirect dimension of methyl ^{1}H-^{13}C correlation spectra (Ottiger et al. 1998; Karamanos et al. 2020) or methyl ^{13}C SQ relaxation dispersion experiments (Lundström et al. 2007), the simplification of the spin-system, previously achieved via selection of the transitions belonging to the $I = 1/2$ manifolds (Tugarinov et al. 2020a), can be accomplished with higher sensitivity through a more straightforward selection of a subset of slow-relaxing (inner) ^{13}C transitions of all methyl manifolds. We show that when this selection is incorporated into a methyl ^{1}H-^{13}C HSQC pulse scheme (Bodenhausen and Ruben 1980), however, the transfer of magnetization from methyl protons to ^{13}C and back to methyl protons for detection, commonly achieved via INEPT schemes (Morris and Freeman 1979) and 90° ^{1}H pulses, becomes suboptimal with respect to attainable sensitivity in the presence of relaxation. The transfer of magnetization to and from the slow-relaxing ^{13}C transitions can be optimized via isolation of slow-relaxing (inner) ^{1}H transitions in conjunction with careful adjustment of the angles of the relevant ^{1}H pulses. This optimized transfer scheme is applied to methyl ^{13}C SQ Carr-Purcell-Meiboom-Gill (CPMG) (Carr and Purcell 1954; Meiboom and Gill 1958) relaxation dispersion experiments (Lundström et al. 2007) recorded on the slow-relaxing methyl ^{13}C transitions of a {U-[^{2}H]; Ileδ1-[$^{13}CH_3$]; Leu,Val-[$^{13}CH_3$,$^{12}CD_3$]}-labeled (ILV-{$^{13}CH_3$}) sample of the ΔST-DNAJB6b deletion mutant of the human DNAJB6b chaperone, a 25-kDa molecular system that undergoes exchange between a major monomeric species and a sparsely populated high-molecular-weight oligomeric species (Karamanos et al. 2019). We show that selection of the slow-relaxing ^{13}C transitions significantly reduces the intrinsic (exchange-free) transverse spin relaxation rates of all exchanging states, and is accompanied by an increase in the information content of the relaxation dispersion profiles for exchanging systems involving high-molecular-weight species (Baldwin et al. 2012).

The energy level diagram of a $^{13}CH_3$ methyl spin system is shown in Figure 1, and consists of one manifold with spin $I = 3/2$ and two manifolds with $I = 1/2$. Vertical and diagonal arrows show a total of 10 SQ ^{1}H and 8 SQ ^{13}C transitions, respectively. In the macromolecular limit, transverse spin relaxation of the inner ^{1}H and ^{13}C transitions of the $I = 3/2$ and $I = 1/2$ manifolds occurs with slower rates ($R^{S}_{2,H}$ and $R^{S}_{2,C}$, shown with red arrows; Figure 1), while the outer ^{1}H and ^{13}C transitions of the $I = 3/2$ manifold are characterized by much faster rates of decay ($R^{F}_{2,H}$ and $R^{F}_{2,C}$, blue arrows) (Tugarinov et al. 2003). Although this is not exactly true (Tugarinov and Kay 2007), the slow relaxation rates of ^{1}H and ^{13}C transitions of the $I = 3/2$ and $I = 1/2$ manifolds are assumed to be equal for the purposes of the following discussion. It is clear from the diagram in Figure 1 that since the

inner ^{13}C transitions of the $I = 3/2$ and $I = 1/2$ manifolds corresponding to ^{1}H eigenstates {|2>, |5>, |7>} and {|3>, |6>, |8>}, respectively, are degenerate (*i.e.* have the same chemical shifts), a quartet of peaks is observed in the ^{13}C dimension of a ^{1}H-coupled HSQC experiment (with a 3:1:1:3 ratio of the quartet peak intensities in the absence of relaxation).

Kontaxis and Bax (2001) previously described a procedure to separate each of the peaks (components) of the ^{13}C quartet. Separating the two slow-relaxing, inner components is much more straightforward considering that the total signal I evolves with time τ as, $I(\tau) = I_0\{3\cos(3\pi J_{CH}\tau) + \cos(\pi J_{CH}\tau)\}$, where J_{CH} is the one-bond ^{1}H-^{13}C scalar coupling in a methyl group, the first term accounts for the evolution of the outer two components, and the second one describes that of the inner (slow-relaxing) components of interest. Adjusting the delay τ to $1/(6J_{CH})$ ensures that angles of 30° and 90° are accrued by the inner and outer components, respectively, allowing one to select for the former with a loss of only $(1 - \sqrt{3}/2) = 0.13$ of initial magnetization. The scheme with this selection implemented before the indirect evolution period (t_1; ^{13}C) of a ^{1}H-^{13}C HSQC experiment, SHSQC, is reproduced for clarity in Figure 2A, with the element selecting for the slow-relaxing ^{13}C transitions enclosed in a solid box. The signal detected at the end of the experiment in Figure 2A, S^{SHSQC}, as a function of the direct (t_2) and indirect (t_1) acquisition times is given by the following four terms (Tugarinov et al. 2003; Tugarinov and Kay 2013),

$$S^{\mathrm{SHSQC}}(t_1,t_2)=\frac{1}{4}\left\{\begin{array}{l}\left[9\exp\left(-2\tau_a R^{\mathrm{F}}_{2,\mathrm{H}}\right)-3\exp\left(-2\tau_a R^{\mathrm{S}}_{2,\mathrm{H}}\right)\right]\exp\left(-2\tau_a R^{\mathrm{F}}_{2,\mathrm{H}}\right)\exp\left(-t_1 R^{\mathrm{S}}_{2,\mathrm{C}}\right)\exp\left(-t_2 R^{\mathrm{F}}_{2,\mathrm{H}}\right)\\ +\left[9\exp\left(-2\tau_a R^{\mathrm{S}}_{2,\mathrm{H}}\right)-3\exp\left(-2\tau_a R^{\mathrm{F}}_{2,\mathrm{H}}\right)\right]\exp\left(-2\tau_a R^{\mathrm{S}}_{2,\mathrm{H}}\right)\exp\left(-t_1 R^{\mathrm{S}}_{2,\mathrm{C}}\right)\exp\left(-t_2 R^{\mathrm{S}}_{2,\mathrm{H}}\right)\end{array}\right\} \quad (1)$$

In the absence of relaxation, $S^{SHSQC} = 3$, as opposed to 12 for the 'full' HSQC scheme (with all transitions included). In the presence of relaxation, however, the transfer of magnetization from methyl ^{1}H to ^{13}C and back to ^{1}H for detection that involve 90° ^{1}H pulses cease to be optimal as we show in detail below.

It is instructive to first consider how each of the components of methyl ^{1}H magnetization to be detected in the end of the SHSQC experiment varies as a function of the angles of the two ^{1}H pulses responsible for the transfer of magnetization to and from ^{13}C nuclei, which are labeled in Figure 2A by α and β, respectively. Note that $\alpha = \beta = 90°$ in the SHSQC scheme. The ^{1}H magnetization detected in the SHSQC experiment is decomposed onto its 'substituents' for angle β varied between 0 to 90° in the absence of relaxation in Figure 2B (with α kept fixed at 90°). When $\beta = 90°$, one-half of the total detected signal represented by the dashed black curve, derives from the fast-relaxing ^{1}H transitions (blue curves), while the other half derives from the slow-relaxing ^{1}H transitions (red and green curves for the transitions of the $I = 3/2$ and $I = 1/2$ manifolds, respectively, and solid black curve for their sum). Although relaxation is not considered in the plots of Figure 2B, it is clear that in the presence of relaxation, this scenario will lead to a fast decay of one half of the ^{1}H

magnetization during the $2\tau_a$ and t_2 periods. This situation can be remedied by selecting the slow-relaxing ^{1}H coherences before acquisition and adjusting the angle β to the maximum of the signal arising from these coherences (the maximum of the black curve in Figure 2B). The loss of signal associated with such a scheme is small even in the absence of relaxation - calculated to be 1/9 of the total signal (*cf.* the maxima of the solid and dashed black curves in Figure 2B), and can be expected to be readily compensated for by slower relaxation of the (remaining) ^{1}H coherences even in small protein molecules.

Perhaps fortuitously, when the slow-relaxing part of the ^{1}H magnetization is selected before acquisition as described above, there is no 'penalty' to be paid for the same selection after the first INEPT period (when methyl ^{1}H magnetization is transferred to ^{13}C at the beginning of the experiment) if the angle α of the corresponding ^{1}H pulse (Figure 2A) is adjusted to an optimal value. This observation can be rationalized by reference to the simpler case of the SHSQC experiment with 90° ^{1}H pulses. If only the magnetization corresponding to the last two terms in Eq. (1) (*i.e.* ^{1}H coherences relaxing slowly during the last $2\tau_a$ and t_2 periods) is retained, then an additional selection for the slow-relaxing ^{1}H magnetization 'on the way' to ^{13}C - *i.e.* elimination of the last, negative term in Eq. (1) - will only increase the observed signal. Figure 2C shows the magnitude of ^{13}C magnetization arising from ^{13}C transitions of the $I = 3/2$ (red) and $I = 1/2$ (green) manifolds for the first point in the indirect dimension ($t_1 = 0$) as a function of the angle α of the ^{1}H pulse following isolation of the slow-relaxing ^{1}H transitions, while the (detected) ^{1}H magnetization at the first point in the acquisition dimension ($t_2 = 0$) when the angle α is adjusted to its optimal value, is shown in Figure 2D as a function of angle β using the same color code as in Figure 2B. Note that there is an (ever so slight, ~1 %) actual gain in signal intensity obtained after the slow-relaxing ^{1}H transitions are selected and the angle α is adjusted to its optimal value before the magnetization is transferred to ^{13}C nuclei (*cf.* the maxima of the solid black curves in Figures 2B and 2D).

Keeping in mind all the considerations discussed above, we proceeded to design a pulse scheme that achieves optimal selection of the slow-relaxing SQ ^{13}C transitions in $^{13}CH_3$ methyl groups (Figure 3A). The experiment starts with selection of the slow-relaxing ^{1}H transitions followed by a ^1H_y α-angle pulse (the element enclosed in the first dashed box in Figure 3A with the α pulse shown in green). As described in more detail in the Supplementary Information, the intensities of the peaks arising from the slow-relaxing ^{13}C transitions after the ^{1}H pulse with angle α, P_S, are given by,

$$P_S = P_S^{3/2} + P_S^{1/2} = (1/2)\left\{8\sin(\alpha) - 9\sin^3(\alpha)\right\} + 2\sin(\alpha) \quad (2)$$

where the first two terms correspond to the two ^{13}C transitions of the $I = 3/2$ manifold ($P_S^{3/2}$), and the last term - to the four ^{13}C transitions of the $I = 1/2$ manifold ($P_S^{1/2}$). Differentiating the expression in Eq. (2) with respect to angle α and equating the derivative to 0, $dP_S/d\alpha = 0$, yields the optimal angle $\alpha_{opt} = \sin^{-1}(2/3) = 41.8°$. For $\alpha = \alpha_{opt}$, the contributions to ^{13}C magnetization from $P_S^{3/2}$ and $P_S^{1/2}$ are the same and equal to 4/3 (corresponding to the intersection point of the red and green curves in Figure 2C).

Subsequently, the magnetization is transferred to ^{13}C nuclei, and the slow-relaxing, inner ^{13}C transitions are isolated before the indirect acquisition period t_1 (the element enclosed in the solid box in Figure 3A). The transfer of magnetization back to protons for detection starts with the $^1H_{\phi 4}$ pulse applied with angle β followed again by selection of the slow-relaxing ^{1}H transitions (the element enclosed in the second dashed box in Figure 3A, with the β-angle pulse shown in red). The signal detected at the end of the experiment, S_S, is given by (see Supplementary Information for details),

$$S_S = 2S_S^{3/2} + S_S^{1/2} = 2(1/4)\left\{8\sin(\beta) - 9\sin^3(\beta)\right\}P_S^{3/2} + \sin(\beta)P_S^{1/2} \quad (3)$$

where the first two terms correspond to the two SQ ^{1}H transitions of the $I = 3/2$ manifold ($S_S^{3/2}$), and the last term to the four SQ ^{1}H transitions of the $I = 1/2$ manifold ($S_S^{1/2}$). Since for $\alpha = \alpha_{opt}$, $P_S^{3/2} = P_S^{1/2} = 4/3$, differentiating the expression in Eq. (3) with respect to β and equating the derivative to 0, $dS_S/d\beta = 0$, gives, $\beta_{opt} = \sin^{-1}(\sqrt{10/27}) = 37.5°$. When the angles α and β are adjusted to their optimal values (α_{opt}; β_{opt}), the total signal S_S is equal to $(40/27)\sqrt{10/3} = 2.7$, *i.e.* more than 90 % of the signal in the SHSQC experiment (equal to 3, see Eq. (1)) is retained in the absence of relaxation.

As the slow-relaxing ^{1}H and ^{13}C transitions are actively isolated and selected for in an optimal manner at each stage of the experiment (before the t_1 and t_2 acquisition periods), the scheme in Figure 3A effectively represents a single-quantum implementation of the methyl-TROSY experiment (Tugarinov et al. 2003) and, as such, is predicted to be more tolerant to transverse spin relaxation than the SHSQC experiment. Figure 3B shows the plots of signal intensities of the first point of the indirect acquisition dimension ($t_1 = 0$) calculated for the scheme in Figure 3A (green), the SHSQC experiment in Figure 2A (red) and the ratio of the two (black), plotted as a function of molecular rotational correlation time τ_C. Note that the red curve follows the expression in Eq. (1) for $t_1 = 0$. Clearly, ~10 % lower sensitivity of the scheme in Figure 3A in the absence of relaxation ($\tau_C \rightarrow 0$) is predicted to transform to sensitivity gains for τ_C values higher than ~2 ns (corresponding to the correlation time of the smallest of folded proteins), reaching close to ~50 % for larger systems (higher τ_C values).

Figure 3C shows histograms of peak intensity ratios obtained for the experiment of Figure 3A and the SHSQC scheme (Figure 2A) for ILV-{$^{13}CH_3$}-labeled ubiquitin at 25 °C (τ_C ~ 5 ns in D_2O; average ratio = 1.12 ± 0.06) and 5 °C (τ_C ~ 11 ns in D_2O; average ratio = 1.17 ± 0.07), and ILV-{$^{13}CH_3$}-ΔST-DNAJB6b at 25 °C ('apparent' τ_C ~ 16 ns and 25 ns for the two independently tumbling domains (Tugarinov et al. 2020b); average ratio = 1.20 ± 0.08 after exclusion of the 9 very flexible methyl sites that do not show sensitivity gains due to only minor relaxation effects). Although these sensitivity gains are quite modest and fall short of those predicted based on the plot in Figure 3B (mainly, due to inclusion of 8 additional RF pulses and relaxation losses during the total of $4\tau_b$ periods in the elements enclosed in dashed boxes in the scheme of Figure 3A), they are realized even for small protein molecules, such as ubiquitin at room temperature, as well as for exchanging systems, such as ΔST-DNAJB6b that undergoes inter-conversion between the major monomeric species and sparsely-populated high-molecular-weight oligomers (Karamanos et al. 2019).

Several applications that would benefit from selection of the slow-relaxing ^{13}C transitions in methyl groups of proteins can be envisaged. For example, the quantitative measurement of methyl ^{1}H-^{13}C residual dipolar couplings in the indirect dimension of ^{1}H-^{13}C correlation spectra, as well as their direct measurements from the splitting of the methyl ^{1}H-^{13}C doublet, can be achieved by sequestering all slow-relaxing ^{13}C transitions and, in principle, do not require isolating transitions of the $I = 1/2$ manifold described by us earlier (Tugarinov et al. 2020a). Here, instead, we focus on methyl ^{13}C SQ CPMG relaxation dispersion measurements (Lundström et al. 2007). Figure 4A shows the pulse-scheme for recording methyl ^{13}C SQ CPMG relaxation dispersion profiles with optimal selection of slow-relaxing ^{13}C transitions using the 'building blocks' developed above for the experiment in Figure 3A. Examples of methyl ^{13}C relaxation dispersion profiles obtained with the scheme in Figure 4A are compared with those recorded using the experiment developed earlier by Lundström et al. (2007) where *all* ^{13}C methyl coherences are present during CPMG delays, in Figure 4B for ILV-{$^{13}CH_3$}-ubiquitin at 5 °C, and in Figure 4C for ILV-{$^{13}CH_3$}-ΔST-DNAJB6b at 15 °C. (Note a temperature of 15 °C was chosen as the dispersions are larger than at 25 °C).

Although sensitivity losses associated with selection of the slow-relaxing ^{13}C transitions are substantial (an average factor of 3.2 was measured for the cross-peaks of both protein samples in favor of the scheme of Lundström et al. (2007) for the reference plane ($T = 0$), while these losses decrease to the average factor of ~1.9 for relaxation delays T of 50 ms and 30 ms for ubiquitin and ΔST-DNAJB6b, respectively, at the highest CPMG frequency), the effective transverse relaxation rates, $R_{2,\text{eff}}$, are significantly lower for the profiles recorded with selection of the slow-relaxing ^{13}C coherences in both proteins. Lower $R_{2,\text{eff}}$ rates translate into longer constant-time CPMG relaxation periods that can be used in these experiments permitting (1) CPMG relaxation dispersion studies of slower exchange processes, as well as (2) better sampling of the relaxation dispersion profiles. In fact, the constant-time relaxation delay T in the experiment of Figure 4A could be increased from 50 to 80 ms for ubiquitin and from 30 to 50 ms for ΔST-DNAJB6b.

For ubiquitin, there are only two methyl sites (Leu50δ2 and Leu56δ2; Figure 4B) that show weak relaxation dispersion (the difference between $R_{2,\text{eff}}$ at 0 and the highest CPMG frequency, $R_{\text{ex}} \sim 2\ \text{s}^{-1}$), reflecting a fast exchange process likely involving inter-conversion between two or more side-chain conformations (Massi et al. 2005). For the C-terminal domain (CTD) of the ΔST-DNAJB6b chaperone, which was shown earlier to be implicated in association with high-molecular-weight oligomeric species comprising 30–40 monomeric units (Karamanos et al. 2019), methyl ^{13}C relaxation dispersions are more abundant. It is important to note that the intrinsic (exchange-free) transverse relaxation rates R_2 are reduced as a result of selection of the slow-relaxing ^{13}C components in both the major, observable (monomeric) species of ΔST-DNAJB6b and the sparsely populated, high-molecular-weight oligomers. The resulting decrease in the population-weighted average R_2 profoundly affects the relaxation dispersion profiles (Baldwin et al. 2012) significantly increasing their exchange-related information content. This is clearly observed for the relaxation dispersion profiles of Ile140δ1, Val165γ2 and Leu185δ2 of ΔST-DNAJB6b which show higher R_{ex} values in the data recorded with selection of the slow-relaxing ^{13}C components (Figure 4C). We note that the profiles obtained with and without selection of the slow-relaxing ^{13}C components can be fitted together using the same parameters of exchange but separate

intrinsic relaxation rates of the involved species. Specifically, while the rate constants of exchange can be shared between the relaxation dispersion profiles recorded with and without selection of the slow-relaxing ^{13}C components, different sets of R_2 values of the major ($R_{2,A}$) and minor, high-molecular-weight ($R_{2,B}$) states are required for analysis of these two types ^{13}C relaxation dispersion experiments. In both cases, however, the same scaling factor was employed between the relaxation rates of interconverting species, $R_{2,B} = 30R_{2,A}$, where $R_{2,A}$ was a free variable parameter in the fit. Such simultaneous best-fits of the CPMG profiles of the four methyl sites of ΔST-DNAJB6b in Figure 4C to a 2-state model of exchange yields an exchange rate $k_{ex} = 1050 \pm 60$ s^{-1} and a fractional population of 4.7 ± 0.4 % for the oligomeric species (200 μM ΔST-DNAJB6b, 15 °C). Considering that no meaningful parameters of exchange could be extracted from the best-fits of the data without selection of the slow-relaxing ^{13}C transitions alone for the same set of methyl sites (blue profiles in Figure 4C), this clearly illustrates the benefits of reduced R_2 (and, hence, $R_{2,eff}$) relaxation rates in CPMG relaxation dispersion experiments that target exchanging systems with at least one high-molecular-weight player.

In summary, a further demonstration of the utility of acute angle pulses in methyl NMR is provided by the design of pulse schemes incorporating optimized selection of the slow-relaxing components of SQ ^{13}C magnetization in $^{13}CH_3$ methyl groups of selectively methyl-protonated, highly deuterated proteins. The optimized selection scheme is more relaxation-tolerant and provides some sensitivity gains in comparison to the experiment where the undesired (fast-relaxing) components of ^{13}C magnetization are simply ‘filtered-out’ of the picture, and only 90° ^{1}H pulses are employed to transfer the magnetization to and from ^{13}C nuclei. We show that isolation of the slow-relaxing components of ^{13}C magnetization results in retrieval of the information content of ^{13}C SQ CPMG relaxation dispersion profiles obscured by high intrinsic relaxation rates (high molecular weights) of one of the species involved in exchange.

Supplementary Material

Refer to Web version on PubMed Central for supplementary material.

Acknowledgement.

We thank Drs. James Baber, Jinfa Ying and Dan Garrett for technical support. This work was supported by the Intramural Program of the National Institute of Diabetes and Digestive and Kidney Diseases, National Institutes of Health (DK029023 to G.M.C.).

References

Baldwin AJ, Walsh P, Hansen DF, Hilton GR, Benesch JL, Sharpe S, Kay LE (2012) Probing dynamic conformations of the high-molecular-weight αB-crystallin heat shock protein ensemble by NMR spectroscopy. J Am Chem Soc 134:15343–15350. [PubMed: 22916679]

Bodenhausen G, Ruben DJ (1980) Natural abundance ^{15}N NMR by enhanced heteronuclear spectroscopy. Chem Phys Lett 69:185–189.

Carr HY, Purcell EM (1954) Effects of diffusion on free precession in nuclear magnetic resonance experiments. Phys Rev 4:630–638.

Karamanos TK, Tugarinov V, Clore GM (2019) Unraveling the structure and dynamics of the human DNAJB6b chaperone by NMR reveals insights into Hsp40-mediated proteostasis. Proc Natl Acad Sci USA 116:21529–21538. [PubMed: 31591220]

Karamanos TK, Tugarinov V, Clore GM (2020) Determining methyl sidechain conformations in a CS-ROSETTA model using methyl ^{1}H-^{13}C residual dipolar couplings. J Biomol NMR 74:111–118. [PubMed: 31950428]

Kontaxis G, Bax A (2001) Multiplet component separation for measurement of methyl ^{13}C-^{1}H dipolar couplings in weakly aligned media. J Biomol NMR 20:77–82. [PubMed: 11430758]

Lundström P, Vallurupalli P, Religa TL, Dahlquist FW, Kay LE (2007) A single-quantum methyl ^{13}C-relaxation dispersion experiment with improved sensitivity. J Biomol NMR 38:79–88. [PubMed: 17464570]

Marion D, Ikura M, Tschudin R, Bax A (1989) Rapid recording of 2D NMR spectra without phase cycling: application to the study of hydrogen exchange in proteins. J Magn Reson 85:393–399.

Massi F, Grey MJ, Palmer AG (2005) Microsecond timescale backbone conformational dynamics in ubiquitin studied with NMR $R_{1\rho}$ relaxation experiments. Protein Sci. 14:735–742. [PubMed: 15722448]

Meiboom S, Gill D (1958) Modified spin-echo method for measuring nuclear relaxation times. Rev Sci Instrum 29:688–691.

Morris GA, Freeman R (1979) Enhancement of nuclear magnetic resonance signals by polarization transfer. J Am Chem Soc 101:760–762.

Ottiger M, Delaglio F, Marquardt JL, Tjandra N, Bax A (1998) Measurement of dipolar couplings for methylene and methyl sites in weakly oriented macromolecules and their use in structure determination. J Magn Reson 134:365–369. [PubMed: 9761712]

Rosenzweig R, Kay LE (2014) Bringing dynamic molecular machines into focus by methyl-TROSY NMR. Annu Rev Biochem 83:291–315. [PubMed: 24905784]

Schütz S, Sprangers R (2020) Methyl TROSYspectroscopy: a versatile NMR approach to study challenging biological systems. Prog Nucl Magn Reson Spectrosc 116:56–84. [PubMed: 32130959]

Shaka AJ, Keeler T, Frenkiel T, Freeman R (1983) An improved sequence for broadband decoupling: Waltz-16. J Magn Reson 52:335–338.

Tugarinov V, Hwang PM, Kay LE (2004) Nuclear magnetic resonance spectroscopy of high-molecular-weight proteins. Annu Rev Biochem 73:107–146. [PubMed: 15189138]

Tugarinov V, Hwang PM, Ollerenshaw JE, Kay LE (2003) Cross-correlated relaxation enhanced ^{1}H-^{13}C NMR spectroscopy of methyl groups in very high molecular weight proteins and protein complexes. J Am Chem Soc 125:10420–10428. [PubMed: 12926967]

Tugarinov V, Karamanos TK, Ceccon A, Clore GM (2020a) Optimized NMR experiments for the isolation of I=1/2 manifold transitions in methyl groups of proteins. Chemphyschem 21:13–19. [PubMed: 31703148]

Tugarinov V, Karamanos TK, Clore GM (2020b) Magic-angle-pulse driven separation of degenerate ^{1}H transitions in methyl groups of proteins: Application to studies of methyl axis dynamics. Chemphyschem 21:1087–1091. [PubMed: 32246547]

Tugarinov V, Kay LE (2007) Separating degenerate ^{1}H transitions in methyl group probes for single-quantum ^{1}H-CPMG relaxation dispersion NMR spectroscopy. J Am Chem Soc 129:9514–9521. [PubMed: 17628064]

Tugarinov V, Kay LE (2013) Estimating side-chain order in [U-^{2}H;$^{13}CH_3$]-labeled high molecular weight proteins from analysis of HMQC/HSQC spectra. J Phys Chem B 117: 3571–3577. [PubMed: 23458382]

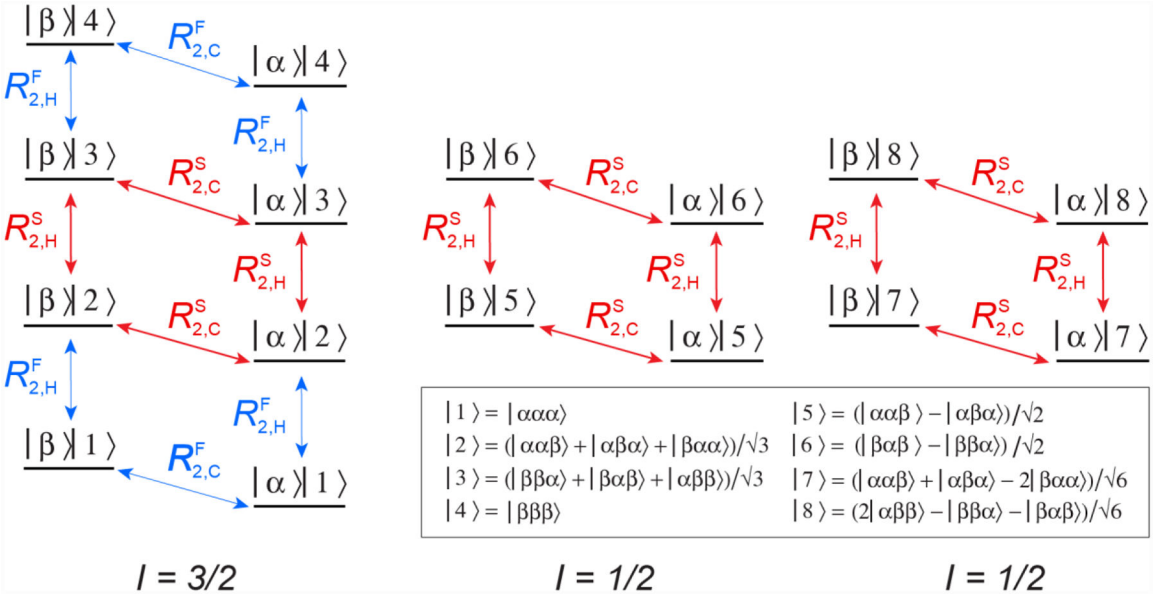

Figure 1.

Energy level diagram of the $^{13}CH_3$ (AX_3) spin-system of a methyl group. Single-quantum ^1H and ^{13}C transitions are shown by vertical and diagonal arrows, respectively. The slow- and fast-relaxing ^1H ($R_{2,H}$) and ^{13}C ($R_{2,C}$) transitions are distinguished by superscripts 'S' and 'F' and shown with red and blue arrows, respectively. The spin quantum numbers, I, of the three manifolds are specified below the energy level diagram. The 16 eigenstates are represented by $|m\rangle|n\rangle$, where $|m\rangle$ is the state of the ^{13}C spin, $m \in \{\alpha,\beta\}$, and the 8 ^1H eigen-states $|n\rangle$ are described by linear combinations of $|i,j,k\rangle$ ($i,j,k \in \{\alpha,\beta\}$). Theoretical expressions for the transverse spin relaxation rates $R_{2,H}$ and $R_{2,C}$ in the macromolecular limit can be found, for example, in (Tugarinov and Kay 2013).

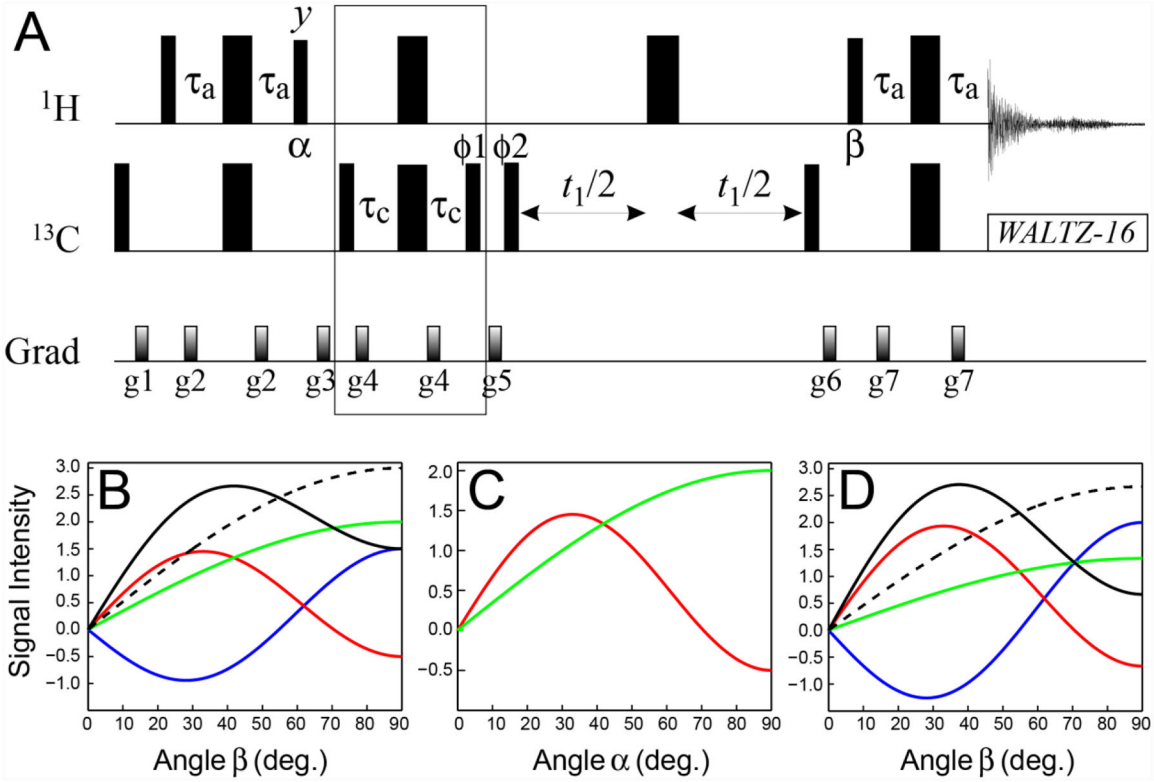

Figure 2.

(**A**) Pulse-scheme for selection of the slow-relaxing ^{13}C transitions in methyl groups (SHSQC). All narrow and wide rectangular pulses are applied with flip angles of 90° and 180°, respectively, along the *x*-axis unless indicated otherwise. The ^{1}H and ^{13}C carrier frequencies are positioned in the center of the Ileδ1-Leu-Val methyl region (0.5 and 20 ppm, respectively). All ^{1}H and ^{13}C pulses are applied with the highest possible power, while ^{13}C WALTZ-16 decoupling (Shaka et al. 1983) is achieved using a 2-kHz field. Delays are: $\tau_a = 1/(4J_{HC}) = 2.0$ ms, $\tau_c = 1/(12J_{HC}) = 0.67$ ms. The durations and strengths of pulsed-field gradients in units of (ms; G/cm) are: g1 = (1; 25), g2 = (0.5; 15), g3 = (1.5; 15), g4 = (0.4; 20), g5 = (1.0; 20), g6 = (0.8; −20), g7 = (0.5; 12). The phase cycle is: ϕ1 = 2(*x*),2(−*x*); ϕ2 = *x*,−*x*; receiver phase = (*x*,−*x*,−*x*,*x*). Quadrature detection in t_1 is achieved via States-TPPI (Marion et al. 1989) incrementation of ϕ2. (**B–D**) Signal intensities (arbitrary units) of the fast-relaxing SQ ^{1}H/^{13}C transitions (blue curves), and the slow-relaxing SQ ^{1}H/^{13}C transitions of the $I = 3/2$ (red curves) and $I = 1/2$ (green curves) manifolds calculated for (**B**) the first direct acquisition point ($t_2 = 0$) of the SHSQC experiment shown in panel A as a function of the angle β (deg.); (**C**) the first point in the indirect (^{13}C) dimension ($t_1 = 0$) as a function of the angle α (deg.) following selection of the slow-relaxing ^{1}H transitions; (**D**) the first direct acquisition point ($t_2 = 0$) as a function of the angle β after selection of the slow-relaxing ^{1}H transitions with an optimal angle α, followed by selection of the slow-relaxing ^{13}C transitions before t_1. In panels (B) and (D) black solid curves show intensities originating from the slow-relaxing ^{1}H and ^{13}C transitions of the sum of the $I = 3/2$ and $I = 1/2$ manifolds, while the dashed black curves show the total signal intensity from all ^{1}H

transitions (including the fast-relaxing ones shown in blue). All calculations were performed in the absence of relaxation.

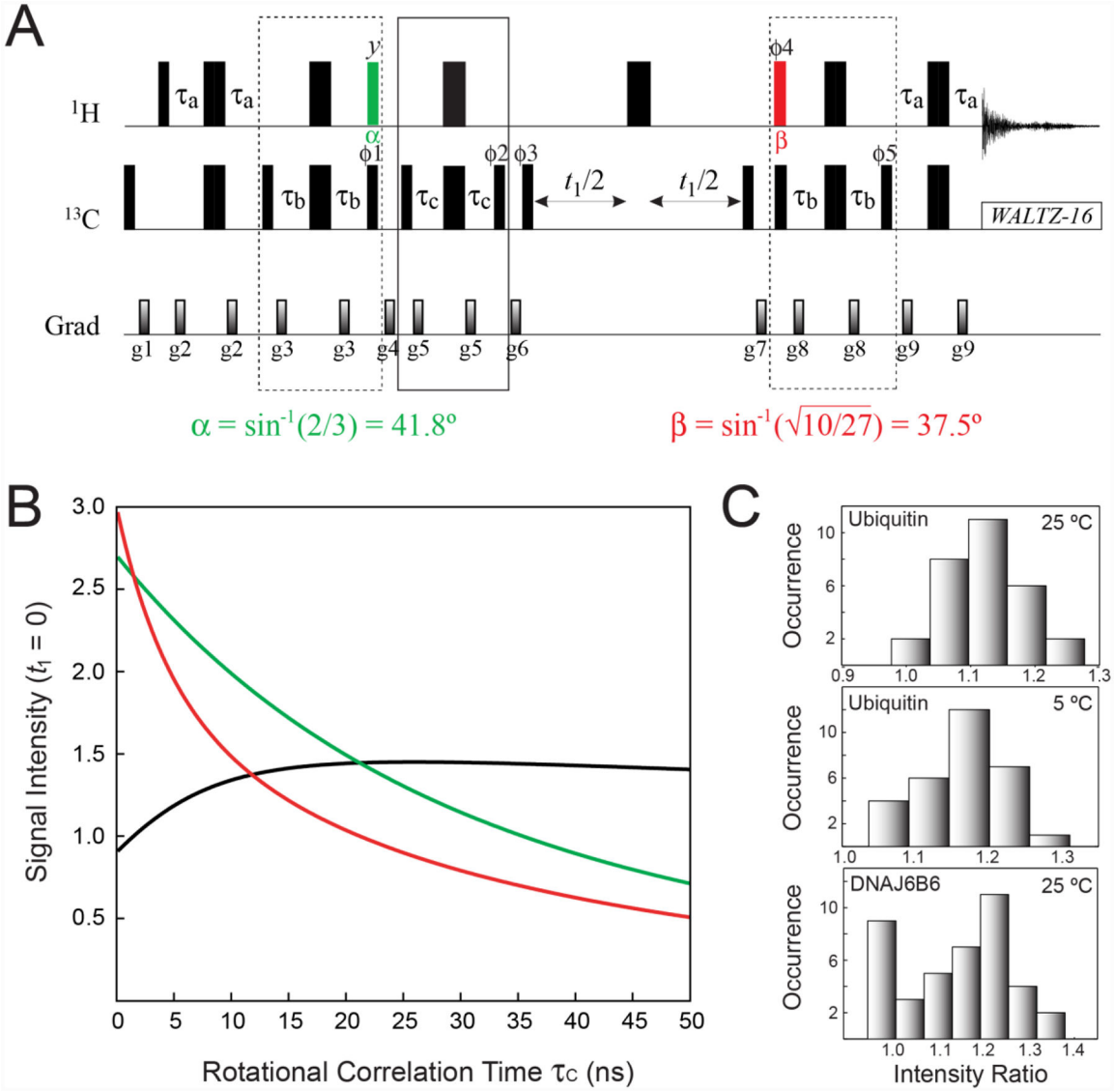

Figure 3.

(**A**) Pulse scheme for the optimal selection of the slow-relaxing ^{13}C transitions in $^{13}CH_3$ methyl groups. All the parameters of the scheme are as described in Figure 2A. The ^{1}H pulse shown in green is applied with flip angle $\alpha = \sin^{-1}(2/3) = 41.8°$, while the pulse shown in red is applied with flip angle $\beta = \sin^{-1}(\sqrt{10/27}) = 37.5°$. The delay $\tau_b = 1/(8J_{HC}) = 1.0$ ms. The durations and strengths of pulsed-field gradients in units of (ms; G/cm) are: g1 = (1; 25), g2 = (0.4; 15), g3 = (0.5; 12), g4 = (0.8; 25), g5 = (0.4; 10), g6 = (1.5; 20), g7 = (0.7; −20), g8 = (0.5; 15), g9 = (0.4; 10). The phase cycle is: ϕ1 = 4(*x*),4(−*x*); ϕ2 = 2(*x*),2(−*x*); ϕ3 = *x*, −*x*; ϕ4 = 4(*x*),4(−*x*); ϕ5 = 4(*x*),4(−*x*); receiver phase = (*x*, −*x*, −*x*,*x*, −*x*,*x*,*x*, −*x*). Quadrature detection in t_1 is achieved via States-TPPI incrementation of ϕ3. (**B**) Signal intensities (arbitrary units) for the first point of the indirect acquisition dimension (t_1 = 0) calculated for the experiment in A (green curve), the SHSQC scheme in Figure 2A (red curve), and the ratio of the two (black curve) plotted as a function of the molecular rotational correlation time τ_C (ns). Expressions for relaxation rates were taken from (Tugarinov and

Kay 2013), with a single external ^{1}H spin placed at a distance of 3.0 Å from methyl protons, and the order parameters of the methyl three-fold axis, S^2_{axis}, set to 0.6. Note that the red curve follows the expression in Eq. (1) for $t_1 = 0$. Calculations were performed using the integral form of $\exp(-R_2 t_2)$ equal to $[1 - \exp(-R_2 t2,\max)]/(R_2 t2,\max)$, where $t_{2,max} = 65$ ms, and R_2 is the transverse relaxation rate of the corresponding ^{1}H transitions (R^{S}_{2H} or R^{F}_{2H}). (**C**) Histograms of experimental peak intensity ratios obtained for the experiment in panel A and the SHSQC experiment (see Figure 2A) for ubiquitin at 5 and 25 °C and the chaperone ΔST-DNAJB6b at 25 °C. Sample conditions and NMR acquisition parameters are described in the ‘Materials and Methods’ section of the Supplementary Information.

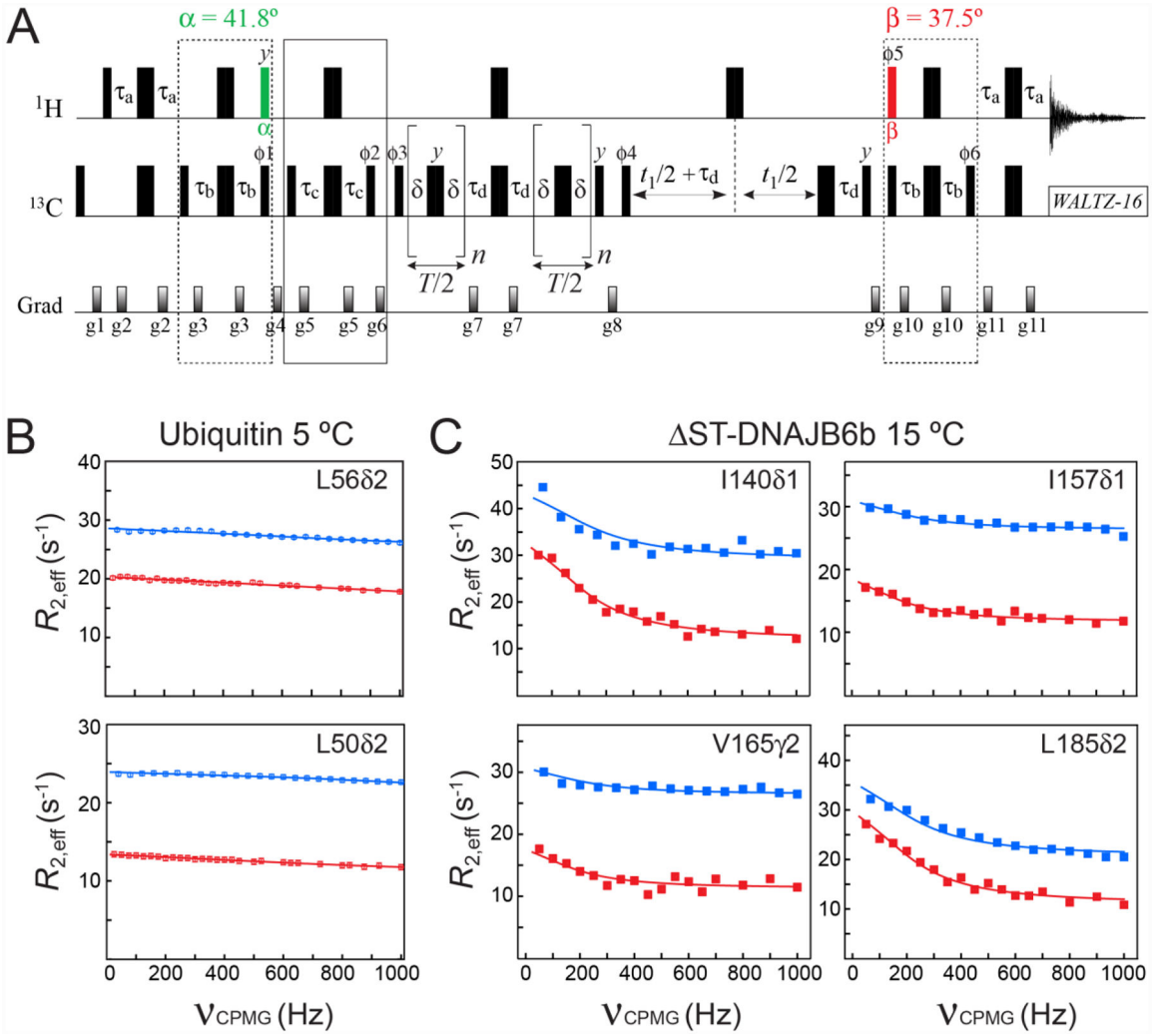

Figure 4.

(**A**) Pulse scheme for methyl ^{13}C SQ CPMG relaxation dispersion experiment with optimal selection of slow-relaxing ^{13}C transitions. All the parameters of the scheme are as described in Figures 2A and 3A. The delay $\tau_d = 1/(4J_{HC}) = 2.0$ ms. T is the CPMG constant time relaxation delay. Even number of CPMG cycles (180° ^{13}C pulses) n should be used for each relaxation period $T/2$. The durations and strengths of pulsed-field gradients in units of (ms; G/cm) are: g1 = (1.0; 25), g2 = (0.5; 15), g3 = (0.3; 20), g4 = (1.5; 25), g5 = (0.25; 15), g6 = (1.2; 20), g7 = (0.5; 20), g8 = (0.6; 20), g9 = (0.8; −25), g10 = (0.3; 20), g11 = (0.5; 20). The phase cycle is: ϕ1 = 8(x),8(−x); ϕ2 = 4(x),4(−x); ϕ3 = 2(x),2(−x); ϕ4 = x,-x; ϕ5 = 8(x),8(−x); ϕ6 = 8(x),8(−x); receiver = (x, −x, −x,x, 2(−x,x,x, −x), x, −x, −x,x). Quadrature detection in t_1 is achieved via States-TPPI incrementation of ϕ4. (**B–C**) Examples of methyl ^{13}C relaxation dispersion profiles obtained for (**B**) ubiquitin at 5 °C, and (**C**) ΔST-DNAJB6b at 15 °C are shown in red. The corresponding profiles obtained with the scheme of Lundström et al. (2007) that does not select the slow-relaxing ^{13}C transitions, are shown in blue. The best fits to a two-state exchange model are shown as continuous lines. In the case of ΔST-DNAJB6b, exchange occurs between the major monomeric state and a sparsely-populated, high-molecular-weight oligomer comprising 30–40 monomeric units (Karamanos et al.

2019). Sample conditions, the parameters of NMR experiments and the details of the fitting procedure are described in the ‘Materials and Methods’ section of the Supplementary Information.